Heliyon 10 (2024) e23352

Contents lists available at ScienceDirect

Heliyon

journal homepage: www.cell.com/heliyon

Biventricular intraventricular mechanical and electrical dyssynchrony in pulmonary arterial hypertension

Wen Li [a], Xian-chang Zhang [b], Yu-ling Qian [a], Xiao-xi Chen [a], Rui-lin Quan [a], Tao Yang [c], Chang-ming Xiong [c], Qing Gu [d], Jian-guo He [c,*]

[a] State Key Laboratory of Cardiovascular Disease, Fuwai Hospital, National Center for Cardiovascular Diseases, Chinese Academy of Medical Sciences and Peking Union Medical College, Beijing, China
[b] MR Collaboration, Siemens Healthineers Ltd., Beijing, China
[c] Center of Pulmonary Vascular Disease, State Key Laboratory of Cardiovascular Disease, Fuwai Hospital, National Center for Cardiovascular Diseases, Chinese Academy of Medical Sciences and Peking Union Medical College, Beijing, China
[d] Emergency Center, State Key Laboratory of Cardiovascular Disease, Key Laboratory of Pulmonary Vascular Medicine, Fuwai Hospital, National Center for Cardiovascular Diseases, Chinese Academy of Medical Sciences, and Peking Union Medical College, Beijing, China

ARTICLE INFO

Keywords:
cardiac magnetic resonance
Electrical dyssynchrony
Intraventricular mechanical dyssynchrony
Pulmonary arterial hypertension
Prognosis

ABSTRACT

Background: Pulmonary arterial hypertension (PAH) leads to myocardial remodeling, manifesting as mechanical dyssynchrony (M-dys) and electrical dyssynchrony (E-dys), in both right (RV) and left ventricles (LV). However, the impacts of layer-specific intraventricular M-dys on biventricular functions and its association with E-dys in PAH remain unclear.

Methods: Seventy-nine newly diagnosed patients with PAH undergoing cardiac magnetic resonance scanning were consecutively recruited between January 2011 and December 2017. The biventricular volumetric and layer-specific intraventricular M-dys were analyzed. The QRS duration *z*-scores were calculated after adjusting for age and sex.

Results: 77.22 % of patients were female (mean age 30.30 ± 9.79 years; median follow-up 5.53 years). Further, 29 (36.71 %) patients succumbed to all-cause mortality by the end of the study. At the baseline, LV layer–specific intraventricular M-dys had apparent transmural gradients compared with RV in the radial and circumferential directions. However, deceased patients lost the transmural gradients. The LV longitudinal strain rate time to late diastolic peak in the myocardial region ($LVmyoLSRTTLDP_{intra}$) predicted long-term survival. The Kaplan–Meier curve revealed that patients with PAH with $LVmyoLSRTTLDP_{intra}$ <20.01 milliseconds had a worse prognosis. Larger right ventricle (RV) intraventricular M-dys resulted in worse RV ejection fraction. However, larger LV intraventricular M-dys in the late diastolic phase indicated remarkable exercise capacity and higher LV stroke volume index. E-dys and intraventricular M-dys had no direct correlations.

Conclusions: The layer-specific intraventricular M-dys had varying impacts on biventricular functions in PAH. PAH patients with $LVmyoLSRTTLDP_{intra}$ <20.01 milliseconds had a worse prognosis. LV intraventricular M-dys in the late diastolic phase needs more attention to precisely evaluate LV function.

* Corresponding author. Address: No.167, Fuwai Hospital, Beilishi Road, Xicheng District, Beijing, 100037, China.
E-mail address: hejianguofw@163.com (J.-g. He).

https://doi.org/10.1016/j.heliyon.2023.e23352
Received 19 July 2023; Received in revised form 16 November 2023; Accepted 1 December 2023
Available online 6 December 2023

1. Introduction

Pulmonary arterial hypertension (PAH) causes right ventricle (RV) afterload increase and myocardial remodeling in both RV and left ventricle (LV) [1], resulting in mechanical dyssynchrony (M-dys) and electrical dyssynchrony (E-dys). The intraventricular M-dys is a nonuniform mechanical contraction and relaxation between ventricular segments [2], resulting in decreased ejection fraction or filling time. Intraventricular M-dys reflects heart function [3,4] and can be calculated through regional time-to-peak myocardial deformation using speckle-tracking echocardiography (STE) or cardiac magnetic resonance (CMR) [5]. Myocardial fibers can deform in 3 spatial directions [6], allowing the intraventricular M-dys evaluation in circumferential, longitudinal, and radial directions. However, the impacts of intraventricular M-dys on biventricular functions in PAH were controversial. The structure and function of myocardium are heterogeneous. Normally, LV has a complex orientation of 3-layer myocardial fibers, including a left-handed helix, a transverse helix, and a right-handed helix in the epicardial, middle, and endocardial layers, respectively [7]. RV myocardial fibers are arranged more circumferentially in the epicardial wall (epiw) and more longitudinally in the endocardial wall (ew), but the middle wall (mw) cannot be properly defined [8]. There is a gradient of strain across the myocardium. In different cardiovascular diseases, the values of layer-specific strain were reported to be different in the aspect of disease diagnosis or prognostic prediction [9]. In PAH, the orientations of myocardial fibers in both LV and RV change [10]. The transmural gradient of M-dys may contribute to better understanding of the physiologic and pathologic characteristics of the heart. The quantification of myocardial fiber deformation in different layers may reflect the changes of ventricles more precisely and detect early impairment of heart function. Therefore, the nonuniform contractions should be evaluated globally and in various myocardial layers to precisely evaluate intraventricular M-dys. However, the layer-specific biventricular intraventricular M-dys in PAH has not been reported earlier. In this study, we presumed that layer-specific biventricular intraventricular M-dys might have various impacts on heart function and help predict prognosis in patients with PAH.

Normal electrical activation is a uniform high-velocity wavefront propagates through the Purkinje network. However, damaged myocardium has altered electrical conduction properties and impairs the velocity and direction of electrical activation [11]. Abnormal depolarization of ventricle results in E-dys, which was quantified by the duration of QRS measured using electrocardiogram (ECG). E-dys negatively impacted LV mechanics in patients with systolic left heart failure [12]. QRS duration correlated with ventricular function but was not a reliable predictor of long-term prognosis in patients with PAH [13,14]. However, the correlation between intraventricular M-dys and E-dys in PAH is unclear. Hill et al. reported no correlation in a pediatric PAH cohort using STE [13], but Badagliacca et al. reported QRS duration as a determinant of RV intraventricular M-dys in adult patients with PAH using STE [15]. Therefore, understanding the correlation between E-dys and intraventricular M-dys in PAH is crucial.

CMR is currently considered the gold standard technique to measure biventricular volumes and function. It is believed to provide more accurate morphological and functional information than echocardiography without radiation [16]. Based on cine CMR images, deformation registration algorithm (DRA)-CMR is a novel post-processing technique for calculating myocardial strain on a pixel basis and analyzing layer-specific intraventricular M-dys [17,18]. However, traditional feature tracking (FT)-CMR can only provide the endocardial and epicardial layer-specific intraventricular M-dys due to its calculation algorithm limitation [9]. Considering the limited spatial resolution (1–2 $\times$ 1–2 mm in-plane resolution, 6- to 8-mm slice thickness) of recent cine CMR techniques [19], RV layer-specific intraventricular M-dys cannot be analyzed using the DRA method in healthy people because of a rather thin RV (3–5 mm in adults) [8]. On the contrary, patients with PAH are suitable candidates considering the hypertrophic RV myocardium. Therefore, this study aimed to illustrate the distribution patterns of layer-specific intraventricular M-dys in both ventricles in a sub-cohort from a prospective PAH registry study [20]. We also wanted to investigate the impact of layer-specific intraventricular M-dys on the long-term prognosis of PAH. Further, we explored the correlations between intraventricular M-dys and E-dys and their impacts on heart function. This study provided a better understanding of M-dys and E-dys in patients with PAH.

2. Methods

2.1. Study population

This investigation was a sub-cohort study from a prospective PAH registry (ClinicalTrials.gov: NCT01417338) [20]. Because CMR was not a routine examination for patients with PAH in our hospital, only patients who agreed to undergo CMR scanning were consecutively recruited between January 2011 and December 2017. Written informed consent was obtained from all enrolled patients. PAH was diagnosed based on the European Society of Cardiology and the European Respiratory Society (ESC/ERS) PH guidelines [21,22]. Right heart catheterization (RHC) was essential for PAH diagnosis. The inclusion and exclusion criteria are illustrated in Supplemental Materials. This study protocol complied with the Declaration of Helsinki and was approved by the Institutional Review Board of Fuwai Hospital (Approval No. 2009–208).

2.2. Right heart catheterization

All included patients underwent RHC at baseline, and the cardiopulmonary hemodynamics were recorded during the examination (see Supplemental Materials).

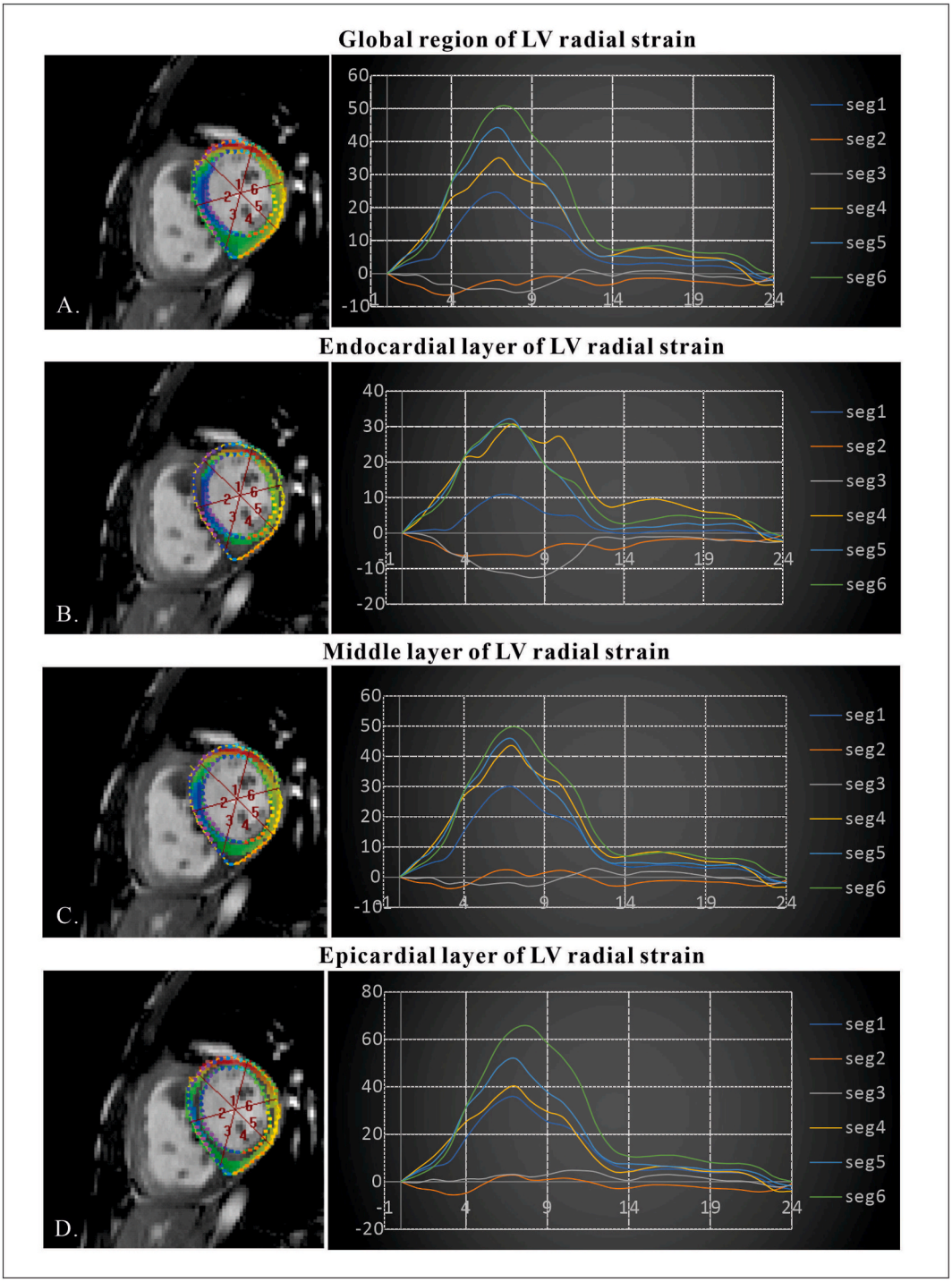

Fig. 1. The analysis of LV global and layer-specific radial strain by DRA-CMR method.
The endocardial and epicardial contours of LV and RV were manually delineated on short-axis cine images at the basal, mid-ventricular, and apical levels, and a slice of the standard four-chamber long-axis cine images. Then, consecutive contours on other phases during the whole cardiac cycle were tracked automatically by Trufi Strain 2.1. Trufi Strain 2.1 would then automatically calculate strain values in the global region and in three layers. Radial strain was quantified on a short axis, with 4 segments delineating the free wall and 2 segments corresponding to the interventricular septum. Fig. 1-A showed the global region of LV radial strain derived from the short-axis cine images and the values of global region of LV radial strain in each segment. Fig. 1-B showed the values of endocardial layer of LV radial strain in each segment. Fig. 1-C showed the values of middle layer of LV radial strain in each segment. Fig. 1-D showed the values of epicardial layer of LV radial strain in each segment.

2.3. ECG

Twelve-lead ECGs (leads I, II, III, aVR, aVL, aVF, V1, V2, V3, V4, V5, V6, Fig. S1) were collected a day before RHC as a part of the clinical routine. Study subjects were resting in a supine position. ECGs were obtained with standard settings of 25 mm/s speed and 10

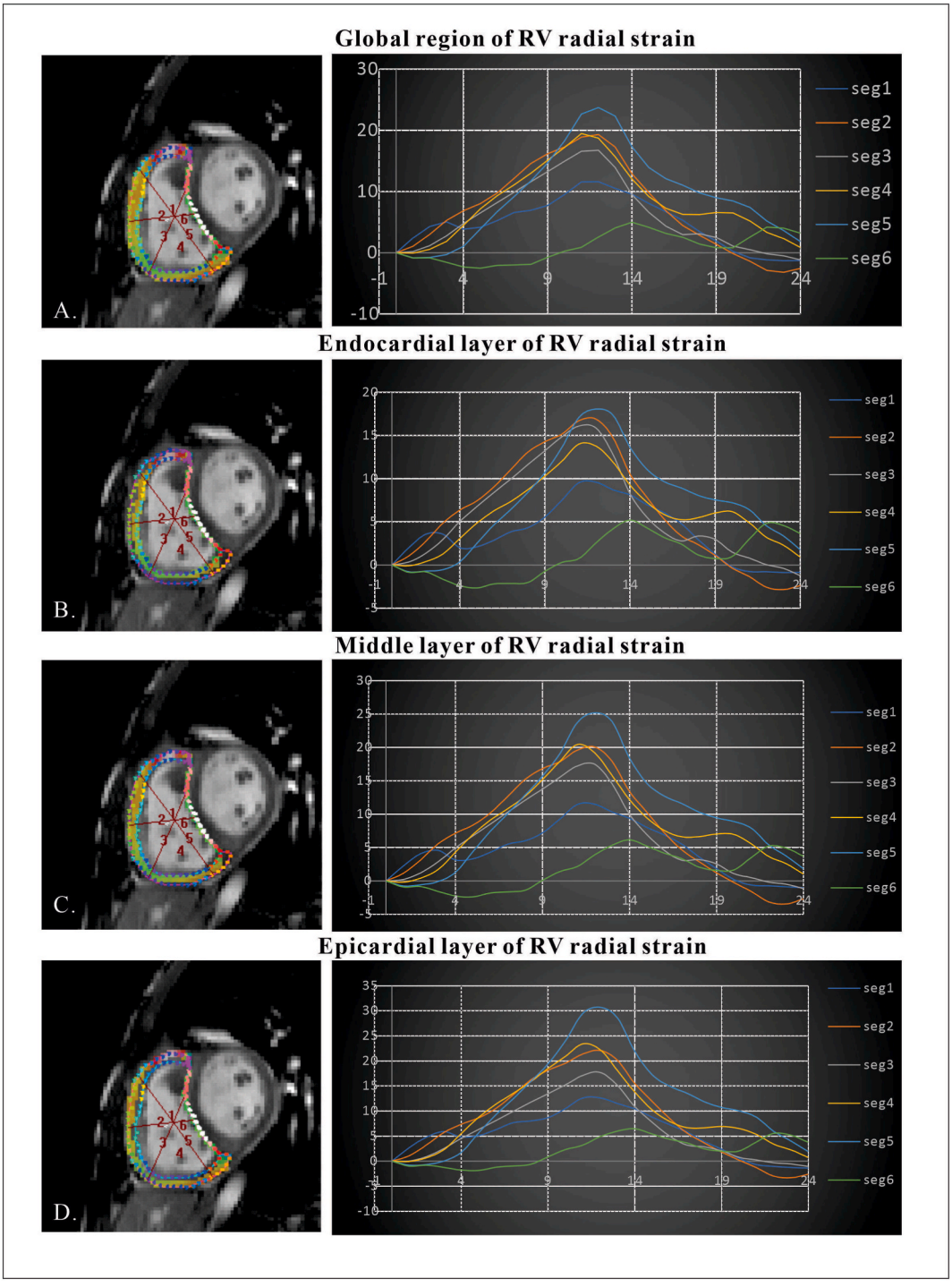

Fig. 2. The analysis of RV global and layer-specific radial strain by DRA-CMR method. A: the global region of RV radial strain derived from the short-axis cine images and the values of global region of RV radial strain in each segment. B: the values of endocardial layer of RV radial strain in each segment. C: the values of middle layer of RV radial strain in each segment. D: the values of epicardial layer of LV radial strain in each segment.

mm/mV amplitude. QRS duration was described as the widest interval in any of the 12 leads and was acquired digitally [23]. The QRS duration-specific z-scores adjusted for sex and age were calculated using the following algorithms [24]. Patients with a QRS z-score ≥ 2 were considered to have E-dys [14].

$$\text{Female}: z = \frac{QRSd - (67 + 1.8\text{age} - 0.046\text{age}^2 + 0.00038\text{age}^3)}{8.1 + 0.20\text{age} - 0.0053\text{age}^2 + 0.000046\text{age}^3}$$

$$\text{Male}: z = \frac{QRSd - (68 + 2.0\text{age} - 0.043\text{age}^2 + 0.00029\text{age}^3)}{8.4 + 0.29\text{age} - 0.0083\text{age}^2 + 0.000076\text{age}^3}$$

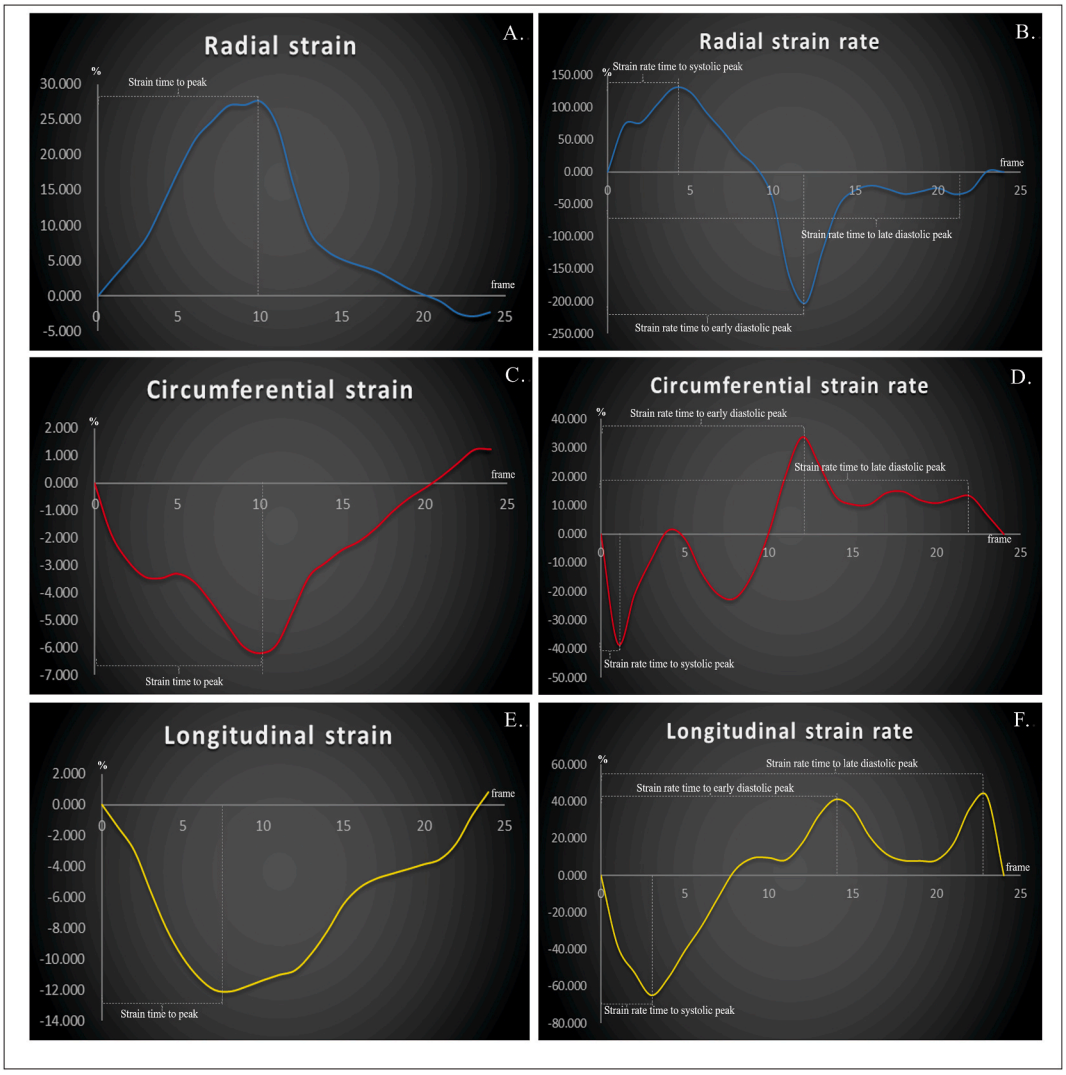

Fig. 3. Schematic diagram of LV strain and strain rate changing curves in the radial, circumferential, and longitudinal directions during a cardiac cycle in patients with PAH.
A, C, and E respectively showed the curves of radial, circumferential, and longitudinal strains during a cardiac cycle. Strain time to peak indicated the period from the start of a cardiac cycle to the point when the strain reached the maximum value. B, D, and F showed the curves of radial, circumferential, and longitudinal strains rate during a cardiac cycle. Strain rate time to systolic peak indicated the period from the start of a cardiac cycle to the point when the strain rate reached the maximum or minimum value during the systolic phase. Strain rate time to early diastolic peak indicated the period from the start of a cardiac cycle to the point when the strain rate reached the maximum or minimum value during the early diastolic phase. Strain rate time to late diastolic peak indicated the period from the start of a cardiac cycle to the point when the strain rate reached the maximum or minimum value during the late diastolic phase.

Table 1
Comparisons of baseline demographics, clinical characteristics and hemodynamics between survivors and deceased PAH patients.

	Total	Survivor	Death	*p*
Patient number	79	50 (63.29 %)	29 (36.71 %)	NA
Follow-up period, days (Q1, Q3)	2018 (1294, 2869)	2464 (1918, 2975)	1068 (709, 1569)	<0.001*
Sex, male (%)	18 (22.78 %)	9 (18.00 %)	9 (31.03 %)	0.266
Age, years	30.30 ± 9.79	30.62 ± 9.25	29.76 ± 10.81	0.709
6MWD, m	411.80 ± 86.03	423.69 ± 93.64	391.23 ± 67.80	0.126
WHO functional class				
I/II, n (%)	41 (51.90 %)	27 (54.00 %)	14 (48.28 %)	0.648
III/IV, n (%)	38 (48.10 %)	23 (46.00 %)	15 (51.72 %)	
Diagnosis				
IPAH/HPAH, n (%)	65 (82.28 %)	42 (84.00 %)	23 (79.31 %)	0.837
CTD-PAH, n (%)	6 (7.59 %)	4 (8.00 %)	2 (6.90 %)	
CHD-PAH, n (%)	8 (10.13 %)	4 (8.00 %)	4 (13.79 %)	
2022 ESC/ERS three-strata risk stratification				
Low risk, n (%)	24 (30.38 %)	20 (40.00 %)	4 (13.79 %)	0.046*
Intermediate risk, n (%)	45 (56.96 %)	25 (50.00 %)	20 (68.97 %)	
High risk, n (%)	10 (12.66 %)	5 (10.00 %)	5 (17.24 %)	
REVEAL Lite 2.0 risk stratification				
Low risk, n (%)	17 (21.52 %)	15 (30.00 %)	2 (6.90 %)	0.024*
Intermediate risk, n (%)	31 (39.24 %)	20 (40.00 %)	11 (37.93 %)	
High risk, n (%)	31 (39.24 %)	15 (30.00 %)	16 (55.17 %)	
Electrical dyssynchrony				
QRS duration, ms	97.54 ± 17.01	97.88 ± 15.84	96.97 ± 19.15	0.820
QRS ≥120 ms	16 (20.25 %)	12 (24.00 %)	4 (13.79 %)	0.277
QRS z-score	0.61 ± 1.45	0.71 ± 1.45	0.45 ± 1.47	0.440
QRS z-score ≥2	13 (16.46 %)	10 (20.00 %)	3 (10.34 %)	0.214
Cardiopulmonary hemodynamics measured by RHC				
Mixed S_VO_2, %	70.56 ± 8.62	71.10 ± 8.95	69.64 ± 8.10	0.471
PaO_2, mmHg	107.24 ± 96.74	113.67 ± 121.58	96.16 ± 1.93	0.442
mRAP, mmHg	5.75 ± 4.87	5.58 ± 5.30	6.03 ± 4.09	0.692
RVSP, mmHg	92.33 ± 26.02	89.06 ± 26.70	97.97 ± 24.24	0.144
RVEDP, mmHg	10.87 ± 7.50	10.60 ± 8.51	11.34 ± 5.43	0.673
sPAP, mmHg	90.97 ± 26.91	87.82 ± 28.52	96.41 ± 23.31	0.173
dPAP, mmHg	41.08 ± 14.67	37.98 ± 13.35	46.41 ± 15.53	0.013*
mPAP, mmHg	59.90 ± 17.67	57.00 ± 16.62	64.90 ± 18.58	0.055
Cardiac index, L/min/m^2	2.96 ± 1.14	3.16 ± 1.27	2.62 ± 0.78	0.042*
PCWP, L/min	7.81 ± 3.35	7.38 ± 3.15	8.55 ± 3.60	0.135
PVR, wood unit	12.20 ± 6.09	11.00 ± 5.61	14.28 ± 6.43	0.020*
Transthoracic echocardiographic indices				
LA diameters, mm	29.33 ± 3.67	29.92 ± 3.33	28.31 ± 4.05	0.060
LV diameters, mm	36.94 ± 5.92	37.84 ± 5.42	35.38 ± 6.51	0.075
LVEF, %	65 ± 6	666 ± 66	63 ± 7	0.083
RV diameters, mm	32.38 ± 6.36	32.60 ± 6.14	32.00 ± 6.84	0.689
Estimated SPAP, mmHg	90.42 ± 24.40	90.57 ± 22.96	90.14 ± 27.17	0.941
Pericardial effusion	7 (8.86 %)	2 (4.00 %)	5 (17.24 %)	0.092
Cardiopulmonary exercise testing				
Peak VO_2, mL/min/kg	13.46 ± 3.77	14.19 ± 4.09	12.11 ± 2.75	0.111
Peak VO_2 pred, %	38.87 ± 11.79	41.47 ± 11.62	33.00 ± 10.20	0.015*
Laboratory tests				
NT-proBNP, pg/ml (Q1, Q3)	856 (521, 1512)	766 (446, 1240)	1108 (639, 1853)	0.237
URIC, umol/L	389.45 ± 115.52	361.03 ± 102.59	438.46 ± 121.77	0.003*
CMR-derived volume metrics				
RVEDVI, ml/m^2	61.22 ± 22.11	60.21 ± 22.28	62.95 ± 22.11	0.598
RVESVI, ml/m^2	51.93 ± 20.80	50.69 ± 21.52	54.06 ± 19.68	0.491
RVSVI, ml/m^2	9.41 ± 5.28	9.71 ± 5.87	8.89 ± 4.16	0.509
RVCI, L/min/m^2	0.68 ± 0.38	0.68 ± 0.41	0.68 ± 0.33	0.979
RVEF, %	16 ± 8	17 ± 10	15 ± 6	0.204
LVEDVI, ml/m^2	29.15 ± 9.33	30.38 ± 9.56	27.04 ± 8.67	0.126
LVESVI, ml/m^2	13.99 ± 5.80	14.33 ± 5.79	13.40 ± 5.86	0.493
LVSVI, ml/m^2	15.16 ± 5.16	16.05 ± 5.56	13.64 ± 4.02	0.030*
LVCI, L/min/m^2	1.11 ± 0.36	1.15 ± 0.38	1.04 ± 0.31	0.182
LVEF, %	53 ± 9	53 ± 10	51 ± 9	0.379
PAH targeted-drug options, n (%)				
ERA	16 (20.25 %)	7 (13.73 %)	9 (31.03 %)	0.044*
PDE5i	43 (54.43 %)	33 (64.70 %)	11 (37.93 %)	
Prostacyclin analogues	2 (2.53 %)	0 (0.00 %)	2 (6.90 %)	
CCB	10 (12.66 %)	7 (13.73 %)	3 (10.34 %)	
None	8 (10.13 %)	4 (7.84 %)	4 (13.80 %)	

*: $p < .05$.
BMI: body mass index; 6MWD: 6-min walk distance; IPAH/HPAH: idiopathic/heritable pulmonary arterial hypertension; CTD-PAH: pulmonary

arterial hypertension associated with connective tissue disease; CHD-PAH: pulmonary arterial hypertension associated with corrected adult congenital heart disease; mixed S_VO_2: mixed venous oxygen saturation; PaO_2: alveolar oxygen partial pressure; mRAP: mean right atrial pressure; RVSP: right ventricular systolic pressure; RVEDP: right ventricular end diastolic pressure; sPAP: systolic pulmonary arterial pressure; dPAP: diastolic pulmonary arterial pressure; mPAP: mean pulmonary arterial pressure; PCWP: pulmonary capillary wedge pressure; PVR: pulmonary vascular resistance; LA: left atrial; LV: left ventricle; LVEF: LV ejection fraction; peak VO_2: peak oxygen uptake values; peak VO_2 pred: peak oxygen uptake predicted values; NT-proBNP: N-terminal brain natriuretic peptide; URIC: uric acid; LDH: lactate dehydrogenase; EDVI: end diastolic volume index; ESVI: end systolic volume index; SVI: stroke volume index; ERA: endothelin receptor antagonists; PDE5i: phosphodiesterase type 5 inhibitors; CCB: calcium channel blockers.

2.4. CMR acquisition

The baseline CMR scanning was performed within 1 week after RHC on a Siemens 1.5-T scanner (MAGNETOM Avanto, Siemens Healthcare, Erlangen, Germany). During this period (median interval: 5 days, range 1–7 days), all enrolled patients were in stable hemodynamic conditions. Breath-hold cine images, in three long axes (two-, three-, and four-chamber) and consecutive short-axis views encompassing the whole LV and RV from the apex to the base, were acquired using a balanced steady-state free-precession (bSSFP) sequence (repetition time/echo time = 3.2 milliseconds/1.6 milliseconds; temporal resolution = 34 milliseconds; flip angle = 60°; field of view = 280 × 340 mm^2; matrix = 150 × 256; voxel size = 1.9 × 1.3 mm^2; slice thickness = 8 mm).

2.5. CMR image analyses

Acquired CMR images were analyzed using DRA-CMR post-processing software (Trufi Strain Demonstrator Version 2.1, Siemens Healthcare). LV and RV volumes were calculated by the software automatically after manually delineating the endocardial and epicardial contours on successive short-axis and 4-chamber long-axis cine images.

Three short-axis slices, namely, basal, mid-ventricular, and apical levels, and a slice of the standard four-chamber long-axis were chosen for strain analysis. LV and RV endocardial and epicardial contours at the end-diastolic phase were delineated manually. Then, consecutive contours on other phases during the whole cardiac cycle were tracked automatically by Trufi Strain 2.1. Trufi Strain 2.1 divided the myocardium (Fig. 1-A and Fig. 2-A) into three equal layers, namely, the endocardial wall (ew, the third of the myocardium closest to the endocardium, Fig. 1-B and Fig. 2-B), middle wall (mw, the middle third of the myocardium wall, Fig. 1-C and Fig. 2-C), and epicardial wall (epiw, the third of the myocardium closest to the epicardium, Fig. 1-D and Fig. 2-D). A segmentation algorithm was used to measure the deformation.

Radial and circumferential strains were quantified on a short axis, with 4 segments delineating the free wall and 2 segments corresponding to the interventricular septum. In addition, the longitudinal strain was measured on the standard four-chamber long-axis view, with 3 segments indicating the free wall and 3 segments indicating septum. As depicted in Fig. 3, strain time to peak (STTP, Fig. 3-A, C, and E), strain rate time to systolic peak (SRTTSP), strain rate time to early diastolic peak (SRTTEDP), and strain rate time to late diastolic peak (SRTTLDP) in the circumferential, longitudinal, and radial directions were calculated (Fig. 3-B, D, and F). The peak strain indicates the maximum value of the strain over all frames. The STTP displays the time at which the maximum strain happens. The SRTTSP displays the time at which the maximum strain rate during systole happens. The SRTTEDP displays the time at which the first maximum strain rate during diastole happens. The SRTTLDP displays the time at which the second maximum strain rate during diastole happens. The intraventricular M-dys in each direction was analyzed by computing the standard deviation (SD) of strain time to peak or strain rate time to peak measures generated for corresponding segments [18]. The transmural gradient of M-dys stands for the difference of M-dys between the epicardial wall and the endocardial wall.

2.6. Study outcomes and follow-up

The follow-up was documented from the date the patients underwent RHC to the occurrence of the primary endpoint. The designed primary endpoint was all-cause mortality, lung transplantation, or atrial septostomy. Each patient was followed up by telephone, as an outpatient, or in the hospital at 6-month ± 2-week intervals. During the follow-up, no patient underwent lung transplantation or atrial septostomy. Notably, no patients were lost to follow-up.

2.7. Statistical analyses

The statistical analyses were performed with SPSS 22.0 (SPSS, Inc., IL, USA). The continuous data were expressed as means ± SD or quartiles (Q1, Q3). The categorical data were expressed as frequencies with percentages (%). For normally distributed continuous variables, the differences between 2 groups were analyzed using the 2-tailed unpaired-sample Student *t*-test, and the differences among the 3 groups were analyzed using the one-way analysis of variance (ANOVA) with Bonferroni correction for multiple comparisons. The chi-squared or Fisher's exact tests were used for categorical variables. We evaluated potential mortality risk factors using the univariate Cox regression analysis. Parameters, with a $P < .05$ univariate level of significance, were included in a backward, stepwise multivariate Cox regression model with 2 parameters at one time. Receiver operating characteristic (ROC) curve analysis was used to establish cutoffs to indicate a higher risk of morbidity. In addition, Kaplan–Meier survival analyses were performed for the cumulative occurrence of the endpoints. A P value $< .05$ indicated a statistically considerable difference.

3. Results

3.1. Demographics, clinical characteristics, and hemodynamics

The study included 79 patients with newly diagnosed PAH, of which 65 had idiopathic/heritable PAH, 6 had PAH associated with connective tissue disease, and 8 had PAH associated with corrected adult congenital heart disease (Table 1). Most enrolled patients were female (77.22 %), with a mean age of 30.30 ± 9.79 years. The median follow-up was 2018 days (range, 26–3990 days). By the end of this study, 29 (36.71 %) patients succumbed to all-cause mortality.

3.2. Baseline layer-specific intraventricular M-dys and survival

For LV layer–specific intraventricular M-dys, clear increasing transmural gradients were observed in the radial STTP ($RSTTP_{intra}$, ew: 103.68 ± 54.91 ms, mw: 92.67 ± 48.85 ms, epiw: 82.91 ± 44.86 ms, $P = .033$) and radial SRTTSP ($RSRTTSP_{intra}$, ew: 70.63 ± 30.89 ms, mw: 58.90 ± 32.29 ms, epiw: 53.58 ± 31.56 ms, $P = .003$) from the epicardial to endocardial walls. In the circumferential direction, descending transmural gradients in the circumferential STTP ($CSTTP_{intra}$, ew: 52.43 ± 30.52 ms, mw: 73.20 ± 46.79 ms, epiw: 91.32 ± 55.57 ms, $P < .001$), circumferential SRTTSP ($CSRTTSP_{intra}$, ew: 37.48 ± 23.20 ms, mw: 43.09 ± 23.17 ms, epiw: 49.78 ± 27.84 ms, $P = .009$), circumferential SRTTEDP ($CSRTTEDP_{intra}$, ew: 41.56 ± 31.87 ms, mw: 49.98 ± 71.90 ms, epiw: 53.33 ± 23.13 ms, $P = .048$), and circumferential SRTTLDP ($CSRTTLDP_{intra}$, ew: 55.53 ± 38.85 ms, mw: 59.74 ± 45.42 ms, epiw: 77.54 ± 49.64 ms, $P = .005$) from the epicardial to endocardial walls within LV (Table 2). When comparing the distribution patterns of intraventricular M-dys between survivors and deceased patients with PAH, it was observed that the survivors still had clear increasing transmural gradients in $RSTTP_{intra}$ and $RSRTTSP_{intra}$ and descending transmural gradients in $CSTTP_{intra}$ and $CSRTTSP_{intra}$ from the epicardial to endocardial walls within LV (Table 3). However, deceased patients lost the transmural gradients in the LV (See Table 3).

For layer-specific intraventricular M-dys, further comparisons revealed that deceased patients had lower LV $CSRTTLDP_{intra}$ in the endocardial wall region (LVewCSRTTLDP$_{intra}$, 62.37 ± 42.76 vs 43.75 ± 27.90 ms, $P = .039$), lower LV longitudinal SRTTLDP

Table 2
Baseline biventricular layer-specific intraventricular mechanical dyssynchrony.

LV	Endocardial wall	Middle wall	Epicardial wall	*p*
Radial				
$RSTTP_{intra}$	103.68 ± 54.91	92.67 ± 48.85	82.91 ± 44.86	0.033*
$RSRTTSP_{intra}$	70.63 ± 30.89	58.90 ± 32.29	53.58 ± 31.56	0.003*
$RSRTTEDP_{intra}$	45.43 ± 22.75	41.09 ± 22.02	41.05 ± 23.14	0.378
$RSRTTLDP_{intra}$	92.83 ± 57.56	83.67 ± 59.53	80.83 ± 56.24	0.396
Circumferential				
$CSTTP_{intra}$	52.43 ± 30.52	73.20 ± 46.79	91.32 ± 55.57	<0.001*
$CSRTTSP_{intra}$	37.48 ± 23.20	43.09 ± 23.17	49.78 ± 27.84	0.009*
$CSRTTEDP_{intra}$	41.56 ± 31.87	49.98 ± 71.90	53.33 ± 23.13	0.048*
$CSRTTLDP_{intra}$	55.53 ± 38.85	59.74 ± 45.42	77.54 ± 49.64	0.005*
Longitudinal				
$LSTTP_{intra}$	20.16 ± 34.82	25.65 ± 37.53	29.95 ± 36.77	0.265
$LSRTTSP_{intra}$	31.04 ± 43.02	25.94 ± 37.70	27.90 ± 41.22	0.746
$LSRTTEDP_{intra}$	33.84 ± 35.96	35.48 ± 35.79	38.77 ± 35.27	0.696
$LSRTTLDP_{intra}$	22.87 ± 57.73	24.51 ± 61.29	33.84 ± 70.99	0.531
RV	**Endocardial wall**	**Middle wall**	**Epicardial wall**	***p***
Radial				
$RSTTP_{intra}$	80.91 ± 45.90	80.30 ± 46.21	74.38 ± 45.17	0.612
$RSRTTSP_{intra}$	82.84 ± 46.92	83.47 ± 42.37	84.06 ± 44.78	0.985
$RSRTTEDP_{intra}$	44.76 ± 24.77	43.67 ± 24.62	43.20 ± 23.00	0.917
$RSRTTLDP_{intra}$	66.10 ± 44.71	65.57 ± 47.27	61.58 ± 43.78	0.790
Circumferential				
$CSTTP_{intra}$	99.35 ± 48.42	100.76 ± 47.03	102.58 ± 42.55	0.907
$CSRTTSP_{intra}$	85.95 ± 41.92	85.90 ± 41.77	85.53 ± 40.53	0.998
$CSRTTEDP_{intra}$	49.44 ± 25.64	50.42 ± 26.12	50.77 ± 27.77	0.948
$CSRTTLDP_{intra}$	65.70 ± 45.20	66.56 ± 43.71	72.17 ± 47.53	0.625
Longitudinal				
$LSTTP_{intra}$	52.75 ± 47.42	64.08 ± 61.34	64.83 ± 61.20	0.354
$LSRTTSP_{intra}$	46.78 ± 57.59	57.94 ± 66.22	53.04 ± 62.54	0.551
$LSRTTEDP_{intra}$	41.66 ± 34.16	43.77 ± 43.70	38.47 ± 32.49	0.683
$LSRTTLDP_{intra}$	37.62 ± 55.80	41.54 ± 56.58	43.24 ± 59.80	0.830

*Significant difference among three myocardial layers, p < .05.
RSTTP: radial strain time to peak; RSRTTSP: radial strain rate time to systolic peak; RSRTTEDP: radial strain rate time to early diastolic peak; RSRTTLDP: radial strain rate time to late diastolic peak; CSTTP: circumferential strain time to peak; CSRTTSP: circumferential strain rate time to systolic peak; CSRTTEDP: circumferential strain rate time to early diastolic peak; CSRTTLDP: circumferential strain rate time to late diastolic peak; LSTTP: longitudinal strain time to peak; LSRTTSP: longitudinal strain rate time to systolic peak; LSRTTEDP: longitudinal strain rate time to early diastolic peak; LSRTTLDP: longitudinal strain rate time to late diastolic peak.

Table 3
LV layer-specific intraventricular mechanical dyssynchrony distribution patterns in survivor and deceased patients.

Survivor	Endocardial wall	Middle wall	Epicardial wall	*p*
Radial				
$RSTTP_{intra}$	100.68 ± 52.34	88.43 ± 46.21	75.80 ± 35.64	0.025*
$RSRTTSP_{intra}$	68.44 ± 27.68	57.75 ± 30.76	53.59 ± 28.98	0.034*
$RSRTTEDP_{intra}$	45.15 ± 22.10	40.27 ± 21.75	40.31 ± 22.80	0.452
$RSRTTLDP_{intra}$	99.10 ± 58.09	85.94 ± 61.68	86.37 ± 60.32	0.462
Circumferential				
$CSTTP_{intra}$	51.11 ± 28.58	70.91 ± 47.61	99.43 ± 59.32	<0.001*
$CSRTTSP_{intra}$	36.71 ± 20.98	41.07 ± 21.66	49.06 ± 25.45	0.025*
$CSRTTEDP_{intra}$	41.80 ± 33.08	61.40 ± 74.62	52.81 ± 20.84	0.134
$CSRTTLDP_{intra}$	62.37 ± 42.76	63.99 ± 49.73	83.38 ± 51.31	0.055
Longitudinal				
$LSTTP_{intra}$	17.32 ± 33.10	26.48 ± 39.83	32.14 ± 37.29	0.161
$LSRTTSP_{intra}$	29.12 ± 40.40	30.30 ± 41.39	27.78 ± 40.45	0.958
$LSRTTEDP_{intra}$	34.41 ± 35.93	35.15 ± 35.58	37.79 ± 35.08	0.894
$LSRTTLDP_{intra}$	33.09 ± 71.85	31.40 ± 69.88	40.19 ± 78.02	0.834
Death	**Endocardial wall**	**Middle wall**	**Epicardial wall**	***p***
Radial				
$RSTTP_{intra}$	108.85 ± 59.69	99.99 ± 53.12	95.17 ± 56.00	0.645
$RSRTTSP_{intra}$	74.39 ± 35.98	60.88 ± 35.23	53.56 ± 36.13	0.086
$RSRTTEDP_{intra}$	45.92 ± 24.23	42.52 ± 22.80	42.33 ± 24.07	0.810
$RSRTTLDP_{intra}$	82.00 ± 55.97	79.76 ± 56.47	71.27 ± 47.90	0.725
Circumferential				
$CSTTP_{intra}$	54.72 ± 34.01	77.17 ± 45.90	77.33 ± 46.09	0.071
$CSRTTSP_{intra}$	38.81 ± 26.94	46.58 ± 25.57	51.02 ± 31.98	0.257
$CSRTTEDP_{intra}$	41.15 ± 30.23	57.53 ± 68.19	54.22 ± 26.99	0.359
$CSRTTLDP_{intra}$	43.75 ± 27.90	52.40 ± 36.46	67.48 ± 45.72	0.056
Longitudinal				
$LSTTP_{intra}$	24.58 ± 37.50	24.33 ± 34.17	26.44 ± 36.29	0.972
$LSRTTSP_{intra}$	34.01 ± 47.37	18.94 ± 30.27	28.09 ± 43.19	0.381
$LSRTTEDP_{intra}$	32.96 ± 36.64	36.02 ± 36.78	40.36 ± 36.18	0.746
$LSRTTLDP_{intra}$	7.03 ± 12.14	13.45 ± 43.04	23.64 ± 57.83	0.327

* Significant difference among three myocardial layers, $p < .05$.
RSTTP: radial strain time to peak; RSRTTSP: radial strain rate time to systolic peak; RSRTTEDP: radial strain rate time to early diastolic peak; RSRTTLDP: radial strain rate time to late diastolic peak; CSTTP: circumferential strain time to peak; CSRTTSP: circumferential strain rate time to systolic peak; CSRTTEDP: circumferential strain rate time to early diastolic peak; CSRTTLDP: circumferential strain rate time to late diastolic peak; LSTTP: longitudinal strain time to peak; LSRTTSP: longitudinal strain rate time to systolic peak; LSRTTEDP: longitudinal strain rate time to early diastolic peak; LSRTTLDP: longitudinal strain rate time to late diastolic peak.

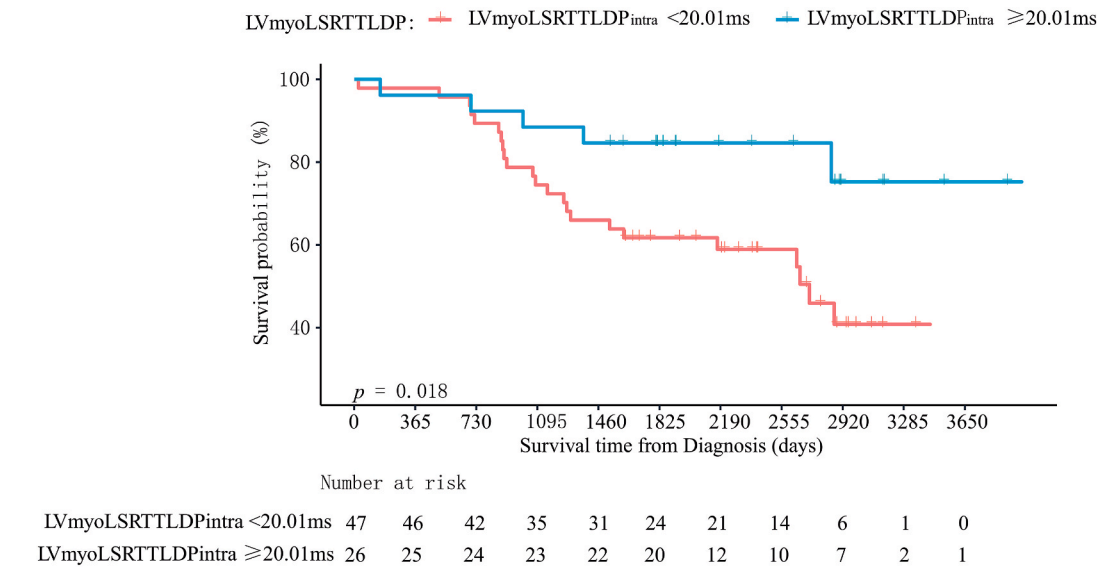

Fig. 4. Kaplan–Meier curve revealed that patients with PAH with $LVmyoLSRTTLDP_{intra}$ <20.01 ms might have a worse prognosis.

($LSRTTLDP_{intra}$) in both the myocardial ($LVmyoLSRTTLDP_{intra}$, 43.64 ± 82.26 vs 6.68 ± 12.51 ms, $P = .005$) and endocardial wall regions ($LVewLSRTTLDP_{intra}$, 33.09 ± 71.85 vs. 7.03 ± 12.14 ms, $P = .021$), and lower RV RSRTTLDP in the myocardial region ($RVmyoRSRTTLDP_{intra}$, 67.98 ± 50.91 vs 48.02 ± 29.30 ms, $P = .030$) (Tables S2 and S3).

The ROC curve analysis revealed that $LVmyoLSRTTLDP_{intra}$ was predictive of long-term survival (AUC: 0.645, $P = .038$, Fig. S4). The Kaplan–Meier curve revealed that patients with PAH with $LVmyoLSRTTLDP_{intra}$ <20.01 ms had a worse prognosis (Fig. 4, log-rank $P = .018$). Multivariate Cox regression analysis revealed that $LVmyoLSRTTLDP_{intra} < 20.01$ ms could still independently predict mortality after adjusting for peak oxygen uptake values (peak VO_2 pred), RHC-RV cardiac index (RVCI), diastolic pulmonary arterial pressure (PAP), or pulmonary vascular resistance (PVR) (Tables S4 and Table 4). $LVmyoLSRTTLDP_{intra}$ ≥20.01 ms had a considerably negative correlation with 2022 ESC/ERC risk stratification ($r = -0.300$, $P = .010$) and NT-proBNP ($r = -0.235$, $P = .045$, Table 5).

LV $RSRTTLDP_{intra}$ in 3 layers had a substantially negative correlation with the World Health Organization Functional Class (WHO-FC), but a considerably positive correlation with 6-min walk distance (6MWD), peak VO_2, CMR-LV end-diastolic volume index (EDVI), and CMR-LV systolic volume index (SVI, Tables S5–S8). RV $RSRTTSP_{intra}$ and $CSRTTSP_{intra}$ in the endocardial and middle walls negatively correlated with CMR-RV ejection fraction (CMR-RVEF, Tables S9–S12).

3.3. Correlation between E-dys and intraventricular M-dys in PAH

In this study, 16 (20.25 %) patients had QRS ≥120 ms (Table 1). When considering E-dys, 13 (16.46 %) patients had a QRS *z*-score ≥2 (Table 6). In addition, patients with PAH with E-dys had higher RV end-diastolic pressure (RVEDP, 9.88 ± 6.00 vs 15.92 ± 11.73 mm Hg, $P = .007$). The QRS *z*-score ≥2 had a considerably positive correlation with RVEDP ($r = 0.301$, $P = .007$), but no remarkable correlation was observed between QRS *z*-score ≥2 and biventricular intraventricular M-dys (Tables S13 and S14).

4. Discussion

The highlights of this study were as follows: (1) The LV layer–specific intraventricular M-dys had noticeable transmural gradients in the radial and circumferential directions compared with RV in patients with PAH. However, deceased patients with PAH lost the transmural gradients of LV layer–specific intraventricular M-dys. (2) patients with PAH with $LVmyoLSRTTLDP_{intra}$ <20.01 ms had a worse long-term prognosis. (3) RV and LV intraventricular M-dys had various impacts on biventricular function. (4) No direct correlations were observed between E-dys and intraventricular M-dys in patients with PAH.

Both LV and RV consist of multilayer myocardial fibers, and each layer has a unique orientation leading to the complex mechanics in both ventricles. The maintenance of normal global function needs appropriate orientations of myocardial layers and regional homogeneity of mechanical shortening and lengthening [25]. The onset of PAH leads to hypertrophy and reorientation of RV myocytes [10], leading to a shift of the RV free wall from a longitudinal to a lateral direction and hence an increase in RV radial contraction [26] and more dependence on transverse wall movement [27]. In addition, the RV dilation causes a prolonged RV post-systolic isovolumetric contraction in the stage when LV is already in the diastolic phase and undergoing early filling [14]. This prolonged RV contraction causes the bulging of the interventricular septum (IVS) into the LV, resulting in a smaller LV and negatively influencing early LV filling [28].

The electrical dyssynchrony of ventricles reflects the abnormal ventricular depolarization. The mechanical dyssynchrony of ventricles can be related to the complex geometry, nonuniform distribution of electric impulses, and heterogeneous activation–inactivation pattern of the sarcomeres [29,30]. However, E-dys, which is manifested as widening QRS duration, is not necessarily related to intraventricular M-dys [29]. In this study, 16.46 % of patients with PAH had a QRS *z*-score ≥2 at the baseline. Although E-dys had close correlations with RVEDP, no direct correlations were observed between E-dys and intraventricular M-dys, consistent with previous findings [13,14]. Therefore, we speculated that the reorientations of myocytes in both ventricles caused a nonuniform contraction, and the analysis of layer-specific intraventricular M-dys in both ventricles in 3 directions might help more precisely assess biventricular mechanics.

In previous studies, the impacts of intraventricular M-dys on biventricular functions in PAH were controversial. A few studies demonstrated that RV intraventricular M-dys in the longitudinal direction measured using echocardiography was associated with

Table 4
Multivariate Cox regression analysis of functional, haemodynamics, and intraventricular mechanical dyssynchrony for total mortality.

	95%CI	*p*
$LVmyoLSRTTLDP_{intra}$<20.02 ms	0.110 (0.014–0.852)	0.035*
Peak VO_2 pred	0.909 (0.851–0.972)	0.005*
$LVmyoLSRTTLDP_{intra}$<20.02 ms	0.367 (0.138–0.973)	0.044*
RHC-RVCI	0.650 (0.408–1.034)	0.069
$LVmyoLSRTTLDP_{intra}$<20.02 ms	0.280 (0.105–0.746)	0.011*
dPAP	1.033 (1.010–1.057)	0.005*
$LVmyoLSRTTLDP_{intra}$<20.02 ms	0.281 (0.105–0.755)	0.012*
PVR	1.097 (1.034–1.163)	0.002*

*: p < .05.
LV: left ventricle; myo: myocardial region; LSRTTLDP: longitudinal strain rate time to late diastolic peak.

Table 5
Correlations between clinical characteristics, hemodynamics, ventricular metrics and LV intraventricular M-dys in myocardial wall.

LV myocardial region	2022 ESC/ERC risk stratification		WHO-FC		SixMWD		peakVO_2		NTproBNP	
	r	p	r	p	r	p	r	p	r	p
$LSRTTLDP_{intra} \geq 20.01$ ms	−0.300	0.010*	−0.022	0.852	0.176	0.157	0.253	0.149	−0.235	0.045*
LV myocardial region	**mRAP**		**RVEDP**		**mPAP**		**RHC-RVCI**		**PVR**	
	r	*p*	*r*	*p*	*r*	*p*	*r*	*p*	*r*	*p*
$LSRTTLDP_{intra} \geq 20.01$ ms	−0.090	0.449	−0.148	0.213	0.138	0.243	0.160	0.177	−0.006	0.963
LV myocardial region	**CMR-RVEDVI**		**CMR-RVESVI**		**CMR-RVSVI**		**CMR-RVCI**		**CMR-RVEF**	
	r	*p*	*r*	*p*	*r*	*p*	*r*	*p*	*r*	*p*
$LSRTTLDP_{intra} \geq 20.01$ ms	−0.113	0.343	−0.156	0.187	0.141	0.233	0.109	0.358	0.172	0.146
LV myocardial region	**CMR-LVEDVI**		**CMR-LVESVI**		**CMR-LVSVI**		**CMR-LVCI**		**CMR-LVEF**	
	r	*p*	*r*	*p*	*r*	*p*	*r*	*p*	*r*	*p*
$LSRTTLDP_{intra} \geq 20.01$ ms	0.001	0.992	−0.085	0.475	0.098	0.410	0.071	0.548	0.145	0.222

*: $p < .05$.
$LSRTTLDP_{intra}$: longitudinal strain rate time to late diastolic peak.

Table 6
Comparisons of baseline demographics, clinical characteristics and hemodynamics between patients with and without electronical dyssynchrony.

	QRS z-score <2	QRS z-score ≥2	*p*
Patient number, n	66 (83.54 %)	13 (16.46 %)	NA
Deceased, n	26 (39.39 %)	3 (23.07 %)	0.353
Sex, male (%)	16 (24.24 %)	2 (15.38 %)	0.721
Age, years	30.76 ± 9.69	28.00 ± 10.38	0.357
6MWD, m	410.40 ± 86.88	419.45 ± 84.85	0.751
QRS ≥120 ms	3 (4.54 %)	13 (100 %)	<0.001*
WHO functional class			
I/II, n (%)	35 (53.03 %)	6 (46.15 %)	0.765
III/IV, n (%)	31 (46.97 %)	7 (53.85 %)	
2022 ESC/ERS three-strata risk stratification			
Low risk, n (%)	21 (31.82 %)	3 (23.08 %)	0.534
Intermediate risk, n (%)	37 (56.06 %)	8 (61.54 %)	
High risk, n (%)	8 (12.12 %)	2 (15.38 %)	
Cardiopulmonary hemodynamics measured by RHC			
Mixed S_VO_2, %	70.58 ± 8.48	70.48 ± 9.69	0.971
PaO_2, mmHg	109.26 ± 105.85	96.99 ± 2.21	0.679
mRAP, mmHg	5.41 ± 4.40	7.46 ± 6.75	0.166
RVSP, mmHg	92.18 ± 25.05	93.08 ± 31.68	0.911
RVEDP, mmHg	9.88 ± 6.00	15.92 ± 11.73	0.007*
sPAP, mmHg	90.35 ± 26.07	94.15 ± 31.83	0.644
dPAP, mmHg	40.45 ± 14.11	44.23 ± 17.56	0.400
mPAP, mmHg	59.15 ± 16.84	63.69 ± 21.76	0.400
Cardiac index, $L/min/m^2$	2.98 ± 1.14	2.84 ± 1.20	0.682
PCWP, L/min	7.82 ± 3.22	7.77 ± 4.07	0.962
PVR, wood unit	11.79 ± 5.61	14.31 ± 8.06	0.174
Cardiopulmonary exercise testing			
Peak VO_2, mL/min/kg	13.67 ± 3.79	12.54 ± 3.84	0.484
Peak VO_2 pred, %	39.32 ± 11.54	36.38 ± 13.65	0.521
CMR volume metrics			
CMR-RVEF, %	16 ± 8	16 ± 11	0.933
CMR-RVEDVI, ml/m^2	59.32 ± 20.42	70.88 ± 28.26	0.085
CMR-RVESVI, ml/m^2	50.31 ± 19.11	60.17 ± 27.29	0.119
CMR-RVSVI, ml/m^2	9.15 ± 4.75	10.71 ± 7.52	0.334
CMR-RVCI, ml/m^2	0.66 ± 0.35	0.81 ± 0.51	0.181
CMR-LVEF, %	52 ± 9	53 ± 12	0.747
CMR-LVEDVI, ml/m^2	29.17 ± 9.68	29.08 ± 7.58	0.975
CMR-LVESVI, ml/m^2	14.08 ± 6.02	13.54 ± 4.69	0.759
CMR-LVSVI, ml/m^2	15.09 ± 5.13	15.54 ± 5.48	0.773
CMR-LVCI, ml/m^2	1.08 ± 0.34	1.22 ± 0.43	0.206

*: $p < .05$.

disease severity [31], had a negative effect on RV systolic pump function [3,4], decreased exercise capacity [32], and was an independent predictor of clinical worsening [15] or clinical events in adult PAH patients [33]. However, Hill et al. reported no correlation between RV intraventricular M-dys (in the longitudinal direction) and hemodynamics or disease severity in pediatric patients with PAH [13]. The study by Kallianos et al. on CMR-pulmonary hypertension (PH) revealed increased LV intraventricular M-dys in the circumferential direction [34]. Jayasekera et al. further reported that LV intraventricular M-dys was impaired in all directions in

idiopathic PAH, and LV intraventricular M-dys in the radial direction independently predicted survival [35].

This study was novel in reporting that the layer-specific intraventricular M-dys had various distribution patterns in both ventricles in patients with PAH. First, LV layer–specific intraventricular M-dys revealed clear transmural gradients in the radial and circumferential directions; however, similar transmural gradients were not observed in RV (Table S1). In addition, deceased patients with PAH lost the transmural gradients of LV layer–specific intraventricular M-dys. We speculated that various orientations of myocardial fibers in the LV and RV might account for the differences in distribution. When the interventricular septum bulged into LV, the right-handed helix (endocardial wall) and transverse myocardial fibers (mid-wall layer) in the LV were influenced more than the left-handed helix (epicardial wall). This deformation of IVS influenced the transmural distribution of contractility, especially in the circumferential and radial directions, which reflected the transverse movements. Studies reported that the transmurally varying properties were necessary to maintain the LV normal pump function [36,37]. Therefore, the disturbance of LV layer–specific intraventricular M-dys transmural gradients in the radial and circumferential directions might reflect an underlying LV dysfunction and indicate a worse prognosis. Stewart et al. reported that, in healthy human hearts, transmural nonuniformity measured using 2D-STE was more pronounced in the LV than in the RV free wall. Endurance training induces transmural remodeling in RV to increase myocardial efficiency [38]. However, in PAH, RV dilation under pressure overload leads to geometric remodeling, which reduces RV contractile efficiency. This explained why the transmural differences in RV intraventricular M-dys were not substantial among various layers.

The present study also demonstrated varying impacts of layer-specific intraventricular M-dys on biventricular functions in patients with PAH. In the RV, a larger intraventricular M-dys in the systolic phase in the radial direction within endocardial and middle walls ($RSRTTSP_{intra}$, Tables S9 and S10) reflected a worse CMR-RVCI and CMR-RVEF, suggesting a negative effect of intraventricular M-dys on RV pump function. This was consistent with previous findings [4,39]. Jayaseker et al. reported that CMR-derived LV intraventricular M-dys reflected by LV radial STTP ($LVRSTTP_{intra}$) negatively correlated with RVEF and positively correlated with RVESV [35]. In addition, they demonstrated that $LVRSTTP_{intra}$ could independently predict survival in patients with idiopathic PAH [35]. $LVmyoRSTTP_{intra}$ also had a considerably positive correlation with NT-proBNP, RVEDP, PVR, RVEDVI, RVESVI, and CMR-RVCI, and a substantially negative correlation with CMR-LVEF in this study, which was consistent with the findings of Jayaseker et al. (Table S8).

In PAH, RV post-systolic isovolumetric contraction and interventricular septum inward movement mainly affect LV mechanics during diastole [14]. Our study observed larger LV intraventricular M-dys in the radial direction in the late diastolic phase within 3 layers ($RSRTTLDP_{intra}$, Tables S5–S8), all reflecting lower WHO-FC, larger CMR-LVEDVI, higher CMR-LVSVI, and remarkable exercise capacity (6MWD and $peakVO_2$). Besides, larger LV intraventricular M-dys in the late diastolic phase in the longitudinal direction ($LVmyoLSRTTLDP_{intra} \geq 20.01$ ms) also indicated lower 2022 ESC/ERC risk stratification, lower NT-proBNP levels, and a better prognosis. According to García et al., in an *in vivo* animal test, increased late systolic LV intraventricular M-dys was associated with impaired LV systolic performance. However, increased diastolic LV intraventricular M-dys was related to delayed ventricular relaxation, reduced LV filling rate, and increased atrial systolic function [29]. Therefore, LV intraventricular M-dys in the systolic and diastolic phases might affect LV function differently. We speculated that the larger LV intraventricular M-dys in the late diastolic phase might result in longer time to filling, contributing to larger LVEDVI and LVSVI. In other words, the intraventricular M-dys in the late diastolic phase in the LV needs more attention.

This study had certain limitations. As a *post hoc* registry analysis, limited patient participation in CMR examinations might have led to selection bias and restricted generalizability. Repeated CMR examinations are necessary to evaluate the reversibility of intraventricular M-dys in both ventricles after PH-targeted drug therapy.

Conclusions

The layer-specific intraventricular M-dys had various distribution patterns and impacts on biventricular function in PAH. PAH patients with $LVmyoLSRTTLDP_{intra} < 20.01$ ms had a worse prognosis. More attention should be paid to the intraventricular M-dys in the late diastolic phase in the LV to evaluate LV function precisely.

Fundings

This study was supported by grants from the National Key Research and Development Program of China, China (No. 2016YFC1304400) and the Youth Foundation of Fuwai Hospital, China (Grant number: 2022-FWQN06).

Data availability statement

Data associated with this study has not been deposited into a publicly available repository. Data will be made available on request.

CRediT authorship contribution statement

Wen Li: Formal analysis, Funding acquisition, Investigation, Methodology, Software, Validation, Writing - original draft, Writing - review & editing. **Xian-chang Zhang:** Methodology, Software, Validation, Visualization, Writing - review & editing. **Yu-ling Qian:** Data curation, Formal analysis, Investigation, Validation, Visualization. **Xiao-xi Chen:** Data curation, Investigation, Validation, Visualization, Writing - review & editing. **Rui-lin Quan:** Investigation, Methodology, Validation, Visualization, Writing - review & editing. **Tao Yang:** Data curation, Investigation, Methodology, Validation, Visualization, Writing - review & editing. **Chang-ming Xiong:** Conceptualization, Investigation, Methodology, Resources, Supervision, Writing - review & editing. **Qing Gu:**

Conceptualization, Investigation, Resources, Supervision, Writing - review & editing. **Jian-guo He:** Conceptualization, Funding acquisition, Methodology, Project administration, Resources, Supervision, Writing - original draft, Writing - review & editing.

Declaration of competing interest

The authors declare that they have no known competing financial interests or personal relationships that could have appeared to influence the work reported in this paper.

Acknowledgments

We gratefully acknowledge Dr. Jens Wetzl (Siemens Healthcare GmbH) for the technical support.

List of nonstandard abbreviations

ANOVA	Analysis of variance
bSSFP	Balanced steady-state free-precession
CI	Cardiac index
CMR	Cardiac magnetic resonance
DRA	Deformation registration algorithm
PAP	Diastolic pulmonary arterial pressure
EF	Ejection fraction
ECG	Electrocardiogram
E-dys	Electrical dyssynchrony
EDVI	End-diastolic volume index
ew	Endocardial wall
ESC/ERS	European Society of Cardiology and the European Respiratory Society
epiw	Epicardial wall
IVS	Interventricular septum
LV	Left ventricle
M-dys	Mechanical dyssynchrony
mw	Middle wall
peak VO_2	Peak oxygen uptake values
PAH	Pulmonary arterial hypertension
PVR	Pulmonary vascular resistance
ROC	Receiver operating characteristic
RHC	Right heart catheterization
RV	Right ventricle
6MWD	Six-minute walk distance
STE	Speckle-tracking echocardiography
SRTTEDP	Strain rate time to early diastolic peak
SRTTLDP	Strain rate time to late diastolic peak
SRTTSP	Strain rate time to systolic peak
STTP	Strain time to peak
$SRTTEDP_{intra}$	Intraventricular M-dys of strain rate time to early diastolic peak
$SRTTLDP_{intra}$	Intraventricular M-dys of strain rate time to late diastolic peak
$SRTTSP_{intra}$	Intraventricular M-dys of strain rate time to systolic peak
$STTP_{intra}$	Intraventricular M-dys of strain time to peak
$CSTTP_{intra}$	Intraventricular M-dys of circumferential strain time to peak
$CSRTTSP_{intra}$	Intraventricular M-dys of circumferential strain rate time to systolic peak
$CSRTTEDP_{intra}$	Intraventricular M-dys of circumferential strain rate time to early diastolic peak
$CSRTTLDP_{intra}$	Intraventricular M-dys of circumferential strain rate time to late diastolic peak
$LSRTTLDP_{intra}$	Intraventricular M-dys of longitudinal strain rate time to late diastolic peak
$RSTTP_{intra}$	Intraventricular M-dys of radial strain time to peak
$RSRTTSP_{intra}$	Intraventricular M-dys of radial strain rate time to systolic peak
$RSRTTLDP_{intra}$	Intraventricular M-dys of radial strain rate time to late diastolic peak
SVI	Systolic volume index
FT	Traditional feature tracking
WHO-FC	World Health Organization Functional Class

Appendix A. Supplementary data

Supplementary data to this article can be found online at https://doi.org/10.1016/j.heliyon.2023.e23352.

References

[1] J. Cao, S. Li, L. Cui, K. Zhu, H. Huo, T. Liu, Biventricular myocardial strain analysis in patients with pulmonary arterial hypertension using cardiac magnetic resonance tissue-tracking technology, J. Clin. Med. 11 (8) (2022) 2230, https://doi.org/10.3390/jcm11082230.

[2] R. Badagliacca, R. Poscia, B. Pezzuto, M. Nocioni, M. Mezzapesa, M. Francone, E. Giannetta, S. Papa, C. Gambardella, S. Sciomer, M. Volterrani, F. Fedele, C. Dario Vizza, Right ventricular remodeling in idiopathic pulmonary arterial hypertension: adaptive versus maladaptive morphology, J. Heart Lung Transplant. 34 (3) (2015) 395–403, https://doi.org/10.1016/j.healun.2014.11.002.

[3] A.P. Kalogeropoulos, V.V. Georgiopoulou, S. Howell, M.A. Pernetz, M.R. Fisher, S. Lerakis, R.P. Martin, Evaluation of right intraventricular dyssynchrony by two-dimensional strain echocardiography in patients with pulmonary arterial hypertension, J. Am. Soc. Echocardiogr. 21 (9) (2008) 1028–1034, https://doi.org/10.1016/j.echo.2008.05.005.

[4] B. Lamia, J.F. Muir, L.C. Molano, C. Viacroze, J. Benichou, P. Bonnet, J. Quieffin, A. Cuvelier, R. Naeije, Altered synchrony of right ventricular contraction in borderline pulmonary hypertension, Int. J. Cardiovasc. Imag. 33 (9) (2017) 1331–1339, https://doi.org/10.1007/s10554-017-1110-6.

[5] F. Leyva, Cardiac resynchronization therapy guided by cardiovascular magnetic resonance, J. Cardiovasc. Magn. Reson. 12 (1) (2010) 64, https://doi.org/10.1186/1532-429X-12-64.

[6] J. Xu, W. Yang, S. Zhao, M. Lu, State-of-the-art myocardial strain by CMR feature tracking: clinical applications and future perspectives, Eur. Radiol. 32 (8) (2022) 5424–5435, https://doi.org/10.1007/s00330-022-08629-2.

[7] F. Triposkiadis, G. Giamouzis, K.D. Boudoulas, G. Karagiannis, J. Skoularigis, H. Boudoulas, J. Parissis, Left ventricular geometry as a major determinant of left ventricular ejection fraction: physiological considerations and clinical implications, Eur. J. Heart Fail. 20 (3) (2018) 436–444, https://doi.org/10.1002/ejhf.1055.

[8] J. Sanz, D. Sánchez-Quintana, E. Bossone, H.J. Bogaard, R. Naeije, Anatomy, function, and dysfunction of the right ventricle: JACC state-of-the-art review, J. Am. Coll. Cardiol. 73 (12) (2019) 1463–1482, https://doi.org/10.1016/j.jacc.2018.12.076.

[9] L. Xu, J.J. Pagano, M.J. Haykowksy, J.A. Ezekowitz, G.Y. Oudit, Y. Mikami, A. Howarth, J.A. White, J.R.B. Dyck, T. Anderson, D.I. Paterson, R.B. Thompson, AB HEART Investigators. Layer-specific strain in patients with heart failure using cardiovascular magnetic resonance: not all layers are the same, J. Cardiovasc. Magn. Reson. 22 (1) (2020) 81, https://doi.org/10.1186/s12968-020-00680-6.

[10] D.W. Park, A. Sebastiani, C.H. Yap, M.A. Simon, K. Kim, Quantification of coupled stiffness and fiber orientation remodeling in hypertensive rat right-ventricular myocardium using 3D ultrasound speckle tracking with biaxial testing, PLoS One 11 (10) (2016), e0165320, https://doi.org/10.1371/journal.pone.0165320.

[11] N.M. Hawkins, M.C. Petrie, M.R. MacDonald, K.J. Hogg, J.J. McMurray, Selecting patients for cardiac resynchronization therapy: electrical or mechanical dyssynchrony? Eur. Heart J. 27 (11) (2006) 1270–1281, https://doi.org/10.1093/eurheartj/ehi826.

[12] S.F. Nagueh, Mechanical dyssynchrony in congestive heart failure: diagnostic and therapeutic implications, J. Am. Coll. Cardiol. 51 (1) (2008) 18–22, https://doi.org/10.1016/j.jacc.2007.08.052.

[13] A.C. Hill, D.M. Maxey, D.N. Rosenthal, S.L. Siehr, S.A. Hollander, J.A. Feinstein, A.M. Dubin, Electrical and mechanical dyssynchrony in pediatric pulmonary hypertension, J. Heart Lung Transplant. 31 (8) (2012) 825–830, https://doi.org/10.1016/j.healun.2012.04.004.

[14] M. Schäfer, K.K. Collins, L.P. Browne, D.D. Ivy, S. Abman, R. Friesen, B. Frank, B. Fonseca, M. DiMaria, K.S. Hunter, U. Truong, J.C. von Alvensleben, Effect of electrical dyssynchrony on left and right ventricular mechanics in children with pulmonary arterial hypertension, J. Heart Lung Transplant. 37 (7) (2018) 870–878, https://doi.org/10.1016/j.healun.2018.01.1308.

[15] R. Badagliacca, M. Reali, R. Poscia, B. Pezzuto, S. Papa, M. Mezzapesa, M. Nocioni, G. Valli, E. Giannetta, S. Sciomer, C. Iacoboni, F. Fedele, C.D. Vizza, Right intraventricular dyssynchrony in idiopathic, heritable, and anorexigen-induced pulmonary arterial hypertension: clinical impact and reversibility, JACC Cardiovasc Imaging 8 (6) (2015) 642–652, https://doi.org/10.1016/j.jcmg.2015.02.009.

[16] A. Pelliccia, S. Caselli, S. Sharma, C. Basso, J.J. Bax, D. Corrado, A. D'Andrea, F. D'Ascenzi, F.M. Di Paolo, T. Edvardsen, S. Gati, M. Galderisi, H. Heidbuchel, A. Nchimi, K. Nieman, M. Papadakis, C. Pisicchio, C. Schmied, B.A. Popescu, G. Habib, D. Grobbee, P. Lancellotti, Internal reviewers for EAPC and EACVI. European Association of Preventive Cardiology (EAPC) and European Association of Cardiovascular Imaging (EACVI) joint position statement: recommendations for the indication and interpretation of cardiovascular imaging in the evaluation of the athlete's heart, Eur. Heart J. 39 (21) (2018) 1949–1969, https://doi.org/10.1093/eurheartj/ehx532.

[17] K. Lin, J.D. Collins, V. Chowdhary, M. Markl, J.C. Carr, Heart deformation analysis for automated quantification of cardiac function and regional myocardial motion patterns: a proof of concept study in patients with cardiomyopathy and healthy subjects, Eur. J. Radiol. 85 (10) (2016) 1811–1817, https://doi.org/10.1016/j.ejrad.2016.08.005.

[18] Y. Li, X. Liu, Y. Xu, W. Li, S. Tang, X. Zhou, J. Sun, Q. Zhang, Y. Han, Y. Chen, The prognostic value of left ventricular mechanical dyssynchrony derived from cardiac MRI in patients with idiopathic dilated cardiomyopathy, Radiol Cardiothorac Imaging 3 (4) (2021), e200536, https://doi.org/10.1148/ryct.2021200536.

[19] A. Schuster, K.N. Hor, J.T. Kowallick, P. Beerbaum, S. Kutty, Cardiovascular magnetic resonance myocardial feature tracking: concepts and clinical applications, Circ Cardiovasc Imaging 9 (4) (2016), e004077, https://doi.org/10.1161/CIRCIMAGING.115.004077.

[20] R. Quan, G. Zhang, Z. Yu, C. Zhang, Z. Yang, H. Tian, Y. Yang, W. Wu, Y. Chen, Y. Liu, X. Zhu, S. Li, J. Shen, Z. Zheng, X. Zhu, G. Wang, Q. Wang, D. Zhou, Y. Ji, T. Yang, W. Li, X. Chen, Y. Qian, Y. Lin, Q. Gu, C. Xiong, G. Shan, J. He, Characteristics, goal-oriented treatments and survival of pulmonary arterial hypertension in China: insights from a national multicentre prospective registry, Respirology 27 (7) (2022) 517–528, https://doi.org/10.1111/resp.14247.

[21] M.M. Hoeper, H.J. Bogaard, R. Condliffe, R. Frantz, D. Khanna, M. Kurzyna, D. Langleben, A. Manes, T. Satoh, F. Torres, M.R. Wilkins, D.B. Badesch, Definitions and diagnosis of pulmonary hypertension, J. Am. Coll. Cardiol. 62 (25 Suppl) (2013) D42–D50, https://doi.org/10.1016/j.jacc.2013.10.032.

[22] N. Galiè, M. Humbert, J.L. Vachiery, S. Gibbs, I. Lang, A. Torbicki, G. Simonneau, A. Peacock, A. Vonk Noordegraaf, M. Beghetti, A. Ghofrani, M.A. Gomez Sanchez, G. Hansmann, W. Klepetko, P. Lancellotti, M. Matucci, T. McDonagh, L.A. Pierard, P.T. Trindade, M. Zompatori, M. Hoeper, ESC scientific document group. 2015 ESC/ERS guidelines for the diagnosis and treatment of pulmonary hypertension: the joint task force for the diagnosis and treatment of pulmonary hypertension of the European society of Cardiology (ESC) and the European respiratory society (ERS): endorsed by: association for European paediatric and congenital Cardiology (AEPC), international society for heart and lung transplantation (ISHLT), Eur. Heart J. 37 (1) (2016) 67–119, https://doi.org/10.1093/eurheartj/ehv317.

[23] X.W. Yang, W. Hua, J. Wang, Z.M. Liu, L.G. Ding, K.P. Chen, S. Zhang, Native QRS narrowing reflects electrical reversal and associates with anatomical reversal in cardiac resynchronization therapy, J. Intervent. Card Electrophysiol. 41 (2) (2014) 161–168, https://doi.org/10.1007/s10840-014-9936-5.

[24] H. Chubb, S.R. Ceresnak, K.S. Motonaga, A.M. Dubin, A proposed method for the calculation of age-dependent QRS duration z-scores, J. Electrocardiol. 58 (2020) 132–134, https://doi.org/10.1016/j.jelectrocard.2019.12.004.

[25] P.P. Sengupta, J. Korinek, M. Belohlavek, J. Narula, M.A. Vannan, A. Jahangir, B.K. Khandheria, Left ventricular structure and function: basic science for cardiac imaging, J. Am. Coll. Cardiol. 48 (10) (2006) 1988–2001, https://doi.org/10.1016/j.jacc.2006.08.030.

[26] E. Pettersen, T. Helle-Valle, T. Edvardsen, H. Lindberg, H.J. Smith, B. Smevik, O.A. Smiseth, K. Andersen, Contraction pattern of the systemic right ventricle shift from longitudinal to circumferential shortening and absent global ventricular torsion, J. Am. Coll. Cardiol. 49 (25) (2007) 2450–2456, https://doi.org/10.1016/j.jacc.2007.02.062.

[27] T. Kind, G.J. Mauritz, J.T. Marcus, M. van de Veerdonk, N. Westerhof, A. Vonk-Noordegraaf, Right ventricular ejection fraction is better reflected by transverse ratxher than longitudinal wall motion in pulmonary hypertension, J. Cardiovasc. Magn. Reson. 12 (1) (2010) 35, https://doi.org/10.1186/1532-429X-12-35.
[28] Y. Yamasaki, M. Nagao, K. Abe, K. Hosokawa, S. Kawanami, T. Kamitani, T. Yamanouchi, K. Horimoto, H. Yabuuchi, H. Honda, Balloon pulmonary angioplasty improves interventricular dyssynchrony in patients with inoperable chronic thromboembolic pulmonary hypertension: a cardiac MR imaging study, Int. J. Cardiovasc. Imag. 33 (2) (2017) 229–239, https://doi.org/10.1007/s10554-016-0985-y.
[29] M.I. Monge García, Z. Jian, F. Hatib, J.J. Settles, M. Cecconi, M.R. Pinsky, Relationship between intraventricular mechanical dyssynchrony and left ventricular systolic and diastolic performance: an in vivo experimental study, Phys. Rep. 11 (4) (2023), e15607, https://doi.org/10.14814/phy2.15607.
[30] F. de Souza Leite, D.E. Rassier, Sarcomere length nonuniformity and force regulation in myofibrils and sarcomeres, Biophys. J. 119 (12) (2020) 2372–2377, https://doi.org/10.1016/j.bpj.2020.11.005.
[31] A. López-Candales, K. Dohi, N. Rajagopalan, M. Suffoletto, S. Murali, J. Gorcsan, K. Edelman, Right ventricular dyssynchrony in patients with pulmonary hypertension is associated with disease severity and functional class, Cardiovasc. Ultrasound 3 (2005) 23, https://doi.org/10.1186/1476-7120-3-23.
[32] R. Badagliacca, S. Papa, G. Valli, B. Pezzuto, R. Poscia, M. Reali, G. Manzi, E. Giannetta, D. Berardi, S. Sciomer, P. Palange, F. Fedele, R. Naeije, C.D. Vizza, Right ventricular dyssynchrony and exercise capacity in idiopathic pulmonary arterial hypertension, Eur. Respir. J. 49 (6) (2017), 1601419, https://doi.org/10.1183/13993003.01419-2016.
[33] M. Murata, T. Tsugu, T. Kawakami, M. Kataoka, Y. Minakata, J. Endo, H. Tsuruta, Y. Itabashi, Y. Maekawa, K. Fukuda, Right ventricular dyssynchrony predicts clinical outcomes in patients with pulmonary hypertension, Int. J. Cardiol. 228 (2017) 912–918, https://doi.org/10.1016/j.ijcard.2016.11.244.
[34] K. Kallianos, G.C. Brooks, K. Mukai, F. Seguro de Carvalho, J. Liu, D.M. Naeger, T. De Marco, K.G. Ordovas, Cardiac magnetic resonance evaluation of left ventricular myocardial strain in pulmonary hypertension, Acad. Radiol. 25 (1) (2018) 129–135, https://doi.org/10.1016/j.acra.2017.07.009.
[35] G. Jayasekera, A. Macdonald, C. Mccomb, V. Orchard, D. Welsh, C. Church, M. Johnson, M. Brewis, C. Berry, A. Radjenovic, A. Peacock, Left ventricular dysfunction and intra-ventricular dyssynchrony in idiopathic pulmonary arterial hypertension, Int. J. Cardiol. 365 (2022) 131–139, https://doi.org/10.1016/j.ijcard.2022.07.032.
[36] H. Wang, X. Zhang, S.M. Dorsey, J.R. McGarvey, K.S. Campbell, J.A. Burdick, J.H. Gorman 3rd, J.J. Pilla, R.C. Gorman, J.F. Wenk, Computational investigation of transmural differences in left ventricular contractility, J. Biomech. Eng. 138 (11) (2016) 1145011–1145016, https://doi.org/10.1115/1.4034558.
[37] S.G. Campbell, P. Haynes, W. Kelsey Snapp, K.E. Nava, K.S. Campbell, Altered ventricular torsion and transmural patterns of myocyte relaxation precede heart failure in aging F344 rats, Am. J. Physiol. Heart Circ. Physiol. 305 (5) (2013) H676–H686, https://doi.org/10.1152/ajpheart.00797.2012.
[38] G.M. Stewart, J. Chan, G.C. Kane, B.D. Johnson, B.N. Balmain, A. Yamada, K. Shiino, L.J. Haseler, S. Sabapathy, Marked disparity in regional and transmural cardiac mechanics in the athlete's heart, Med. Sci. Sports Exerc. 52 (9) (2020) 1908–1914, https://doi.org/10.1249/MSS.0000000000002336.
[39] R. Badagliacca, R. Poscia, B. Pezzuto, S. Papa, C. Gambardella, M. Francone, M. Mezzapesa, M. Nocioni, A. Nona, R. Rosati, S. Sciomer, F. Fedele, C. Dario Vizza, Right ventricular dyssynchrony in idiopathic pulmonary arterial hypertension: determinants and impact on pump function, J. Heart Lung Transplant. 34 (3) (2015) 381–389, https://doi.org/10.1016/j.healun.2014.06.010.